2011

Time-Resolved Resonance Raman and Computational Investigation of the Influence of 4-Acetamido and 4-N-Methylacetamido Substituents on the Chemistry of Phenylnitrene

Jiaden Xue, *University of Hong Kong*
Shubham Vyas, *The Ohio State University*
Yong Du, *University of Hong Kong*
Hoi-Ling Luk, *The Ohio State University*
Yung-Ping Chuang, *University of Hong Kong*, et al.

THE JOURNAL OF PHYSICAL CHEMISTRY A

ARTICLE

pubs.acs.org/JPCA

Time-Resolved Resonance Raman and Computational Investigation of the Influence of 4-Acetamido and 4-*N*-Methylacetamido Substituents on the Chemistry of Phenylnitrene

Jiadan Xue,[†] Shubham Vyas,[‡] Yong Du,[†] Hoi Ling Luk,[‡] Yung Ping Chuang,[†] Tracy Yuen Sze But,[†] Patrick H. Toy,[†] Jin Wang,[‡] Arthur H. Winter,[‡] David Lee Phillips,[*,†] Christopher M. Hadad,[*,‡] and Matthew S. Platz[*,‡]

[†]Department of Chemistry, The University of Hong Kong, Pokfulam Road, Hong Kong S.A.R., People's Republic of China

[‡]Department of Chemistry, The Ohio State University, 100 West 18th Avenue, Columbus, Ohio 43210, United States

Supporting Information

ABSTRACT: A time-resolved resonance Raman (TR^3) and computational investigation of the photochemistry of 4-acetamidophenyl azide and 4-*N*-methylacetamidophenyl azide in acetonitrile is presented. Photolysis of 4-acetamidophenyl azide appears to initially produce singlet 4-acetamidophenylnitrene which undergoes fast intersystem crossing (ISC) to form triplet 4-acetamidophenylnitrene. The latter species formally produces 4,4′-bisacetamidoazobenzene. RI-CC2/TZVP and TD-B3LYP/TZVP calculations predict the formation of the singlet nitrene from the photogenerated S_1 surface of the azide excited state. The triplet 4-acetamidophenylnitrene and 4,4′-bisacetamidoazobenzene species are both clearly observed on the nanosecond to microsecond time-scale in TR^3 experiments. In contrast, only one species can be observed in analogous TR^3 experiments after photolysis of 4-*N*-methylacetamidophenyl azide in acetonitrile, and this species is tentatively assigned to the compound resulting from dimerization of a 1,2-didehydroazepine. The different photochemical reaction outcomes for the photolysis of 4-acetamidophenyl azide and 4-*N*-methylacetamidophenyl azide molecules indicate that the 4-acetamido group has a substantial influence on the ISC rate of the corresponding substituted singlet phenylnitrene, but the 4-*N*-methylacetamido group does not. CASSCF analyses predict that both singlet nitrenes have open-shell electronic configurations and concluded that the dissimilarity in the photochemistry is probably due to differential geometrical distortions between the states. We briefly discuss the probable implications of this intriguing substitution effect on the photochemistry of phenyl azides and the chemistry of the related nitrenes.

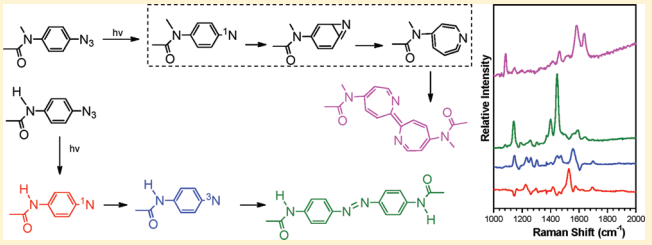

INTRODUCTION

The photochemistry of aryl azides has been extensively studied and laser flash photolysis experiments have enabled direct investigation of the reaction intermediates so produced, as well as the stable photoproducts. This has led to a much improved understanding of reaction mechanisms.[1−60] A singlet arylnitrene species and a nitrogen molecule are typically produced upon photolysis of aryl azides in room temperature solution, and this singlet arylnitrene may then undergo very rapid ring expansion reactions to form 1,2-didehydroazepines (cyclic ketenimines) or decay by intersystem crossing (ISC) to form triplet arylnitrene species.[55] The ring expansion rates of singlet arylnitrenes increase with increasing temperature, but the ISC rates are relatively independent of temperature. Some electron-donating groups in the para position of singlet arylnitrenes have been reported to greatly accelerate the ISC rate. For example, singlet phenylnitrene decays to the lower energy triplet state with a time constant of about $(3.2 \pm 0.3) \times 10^6\ s^{-1}$, but the ISC rate of *p*-dimethylaminophenylnitrene is $(8.3 \pm 0.2) \times 10^9\ s^{-1}$, which is much greater than the rate of its ring expansion in room temperature solution.[52,61]

Certain singlet nitrenes can even react with water to form arylnitrenium ions such as the short-lived arylnitrenes with para-substituted electron-donating groups.[26,28,31−37,40,47,48,61] The 4-*N*-methylacetamido and 4-acetamido substituents on the phenylnitrenium ions have been found to significantly stabilize these two related arylnitrenium ions. These ions have lifetimes of several milliseconds in room temperature solutions.[62,63] Density functional theory (DFT) calculations of these two arylnitrenium ions revealed that the *N*-methyl substitution on the acetamido group has little effect on the structure and properties of arylnitrenium ion and both species had similar iminocyclohexadienyl character.[63] However, there are relatively few studies of the influence of the acetamido and *N*-methylacetamido groups on

Received: February 24, 2011
Revised: May 4, 2011
Published: June 07, 2011

Scheme 1

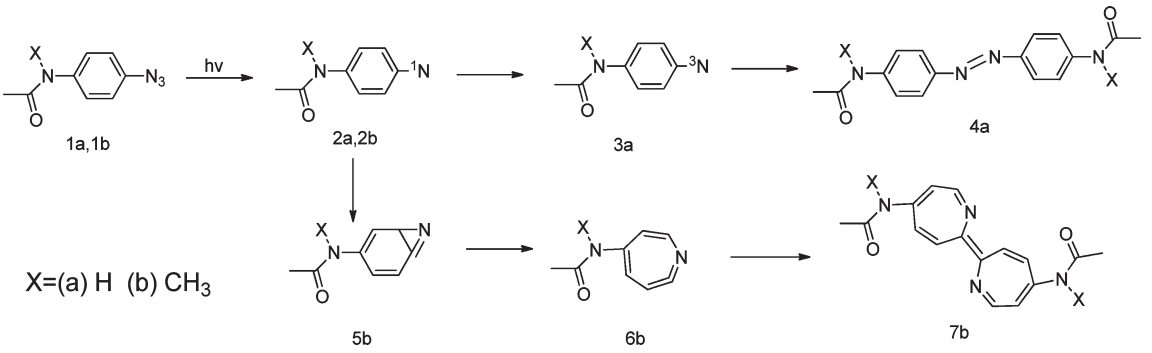

phenylnitrenes. We have recently reported time-resolved resonance Raman (TR^3) spectra for several arylnitrenes and their subsequent reactions.[60a,b,64] In this paper, we present a nanosecond TR^3 study of 4-acetamido- and 4-*N*-methylacetamidophenylnitrenes (**2a**, **2b**) (Scheme 1) in an organic solvent. The TR^3 spectra show that acetamido and *N*-methylacetamido substitutions lead to very different photochemical outcomes for the two substituted phenylnitrenes generated from photolysis of the azide precursors. The singlet 4-acetamidophenylnitrene **2a** was observed to give a triplet nitrene **3a** which then formed the corresponding azo compound, 4,4′-bisacetamidoazobenzene (**4a**). The triplet 4-acetamidophenylnitrene (**3a**) and 4,4′-bisacetamidoazobenzene species (**4a**) were both clearly observed during the TR^3 experiments, and characterized using resonance Raman spectroscopy. In contrast, after photolysis of 4-*N*-methylacetamidophenyl azide (**1b**), only one species was observed on the nanosecond to microsecond time scale, and it was assigned to **7b** formed from dimerization of ring-expansion intermediates, 1,2-didehydroazepines (**6b**). These results strongly suggest that the 4-acetamido substituent has a substantial influence on the ISC rate of the substituted singlet phenylnitrene, but the 4-*N*-methylacetamido group does not.

EXPERIMENTAL AND COMPUTATIONAL METHODS

Samples of 4-acetamidophenyl azide, 4-*N*-methylacetamidophenyl azide, and 4,4′-bisacetamidoazobenzene were synthesized according to literature methods.[62] Solutions of these two phenyl azides were prepared with concentrations of 2 mM or/and 1 mM azide in acetonitrile for the nanosecond TR^3 (ns-TR^3) experiments. Spectroscopic grade acetonitrile was used in preparing the sample solutions.

The experimental apparatus and methods used for the ns-TR^3 experiments have been detailed elsewhere,[60,63−66] so only a brief account will be given here. The fourth harmonic of a Nd:YAG nanosecond pulsed laser system provided the 266 nm laser as pump and 319.9 nm as probe (the third anti-Stokes hydrogen Raman shifted laser line of the 532 nm second harmonic) wavelengths used in the ns-TR^3 experiments. The ns-TR^3 experiments used two Nd:YAG lasers electronically synchronized to each other by a pulse delay generator employed to control the relative timing of the two lasers. A fast photodiode whose output was displayed on a 500 MHz oscilloscope was used to measure the relative timing of the pump and probe pulses with the jitter between the pump and probe pulses determined to be <5 ns. The laser beams were loosely focused onto a flowing liquid stream of sample using a near collinear geometry and the scattered Raman light was collected employing reflective optics and a back scattering geometry. The collected Raman light was imaged through a depolarizer mounted on the entrance of a monochromator that dispersed the light onto a liquid nitrogen cooled CCD detector that collected the Raman signal for 30−60 s before data transfer to an interfaced PC computer. About 10−20 of these readouts were summed to obtain the resonance Raman spectrum. The TR^3 spectra were obtained by subtracting the pump−probe spectrum at negative 100 ns from pump−probe spectra acquired at positive time delays in order to remove the solvent and precursor Raman bands. The known Raman wavenumbers[77] of acetonitrile were used to calibrate the frequencies of the TR^3 spectra to an estimated accuracy of ±5 cm^{-1}. A Lorentzian function was used to integrate the relevant Raman bands in the TR^3 spectra in order to determine their areas and to extract the decay and growth of the species observed in the experiments. During the experiments, no noticeable degradation was observed for the sample by UV/vis absorption spectroscopy.

All of the density functional theory calculations presented here, in particular, for Raman frequencies, were performed using the Gaussian 98 program suite[67] operated on the High Performance Computing clusters installed at the University of Hong Kong or the Ohio Supercomputer Center. Complete geometry optimization and vibrational frequency calculations were analytically performed using the (U)B3LYP method with the 6-31G* basis set for the ground states with the lowest energy configurations obtained for the triplet 4-acetamidophenylnitrene, 4,4′-bisacetamidoazobenzene, and 4-*N*-methylacetamido substituted dimer formed from the 1,2-didehydroazepines. A Lorentzian function with a 20 cm^{-1} bandwidth was employed with the calculated Raman vibrational frequencies and relative intensities to obtain the (U)B3LYP/6-31G* computed Raman spectra reported in this paper.

To investigate the photolysis of the azides and to characterize the singlet excited states, we performed ground and excited state calculations with second-order coupled cluster calculations with the resolution-of-the-identity approximation (RI-CC2)[68] and time-dependent density functional theory, using Becke's three parameter exchange functional along with the Lee−Yang−Parr correlation functional (TD-B3LYP)[69] method with the triple-ζ valence polarized (TZVP)[70] basis sets using the Turbomole-5.91 program.[71] Ground-state geometries of both 4-acetamidophenyl and 4-*N*-methylacetamidophenyl azide were optimized at the RI-CC2/TZVP and TD-B3LYP/TZVP levels of theory. Calculations of vertical excitations followed by evaluation of the gradients for the Franck−Condon excited states were performed to

Table 1. Calculated Vertical Excitations for 4-Acetamidophenyl and 4-*N*-Methylacetamidophenyl Azide

	RI-CC2/TZVP			TD-B3LYP/TZVP		
excited state	wavelength (nm)	oscillator strength	orbital contributions	wavelength (nm)	oscillator strength	orbital contributions
			4-Acetamidophenyl Azide (**1a**)			
1	292	1.1×10^{-3}	46 → 48	334	2.0×10^{-4}	46 → 48
2	266	4.8×10^{-2}	46 → 49	280	2.7×10^{-1}	46 → 47
			46 → 47			46 → 49
			4-*N*-Methylacetamidophenyl Azide (**1b**)			
1	289	9.3×10^{-4}	50 → 52	330	4.0×10^{-4}	50 → 51
2	262	1.8×10^{-2}	50 → 53	276	2.6×10^{-1}	50 → 52
						50 → 53

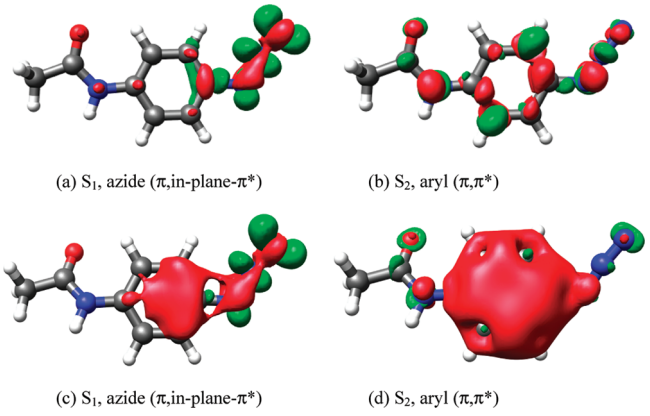

Figure 1. Difference density plots for 4-acetamidophenyl azide (**1a**) at the TD-B3LYP/TZVP, (a) S_1 and (b) S_2, and at the RI-CC2/TZVP, (c) S_1 and (d) S_2, levels of theory. (The green contours depict the accumulation of electron density in the excited state, and the red contours illustrate the loss of electron density from the S_0 ground state. The isocontour values are adjusted differently for appropriate visualization: TD-B3LYP, S_1 ±0.005, S_2 ±0.002; RI-CC2, S_1 −0.02, +0.005; S_2 −0.01, +0.0005 au.)

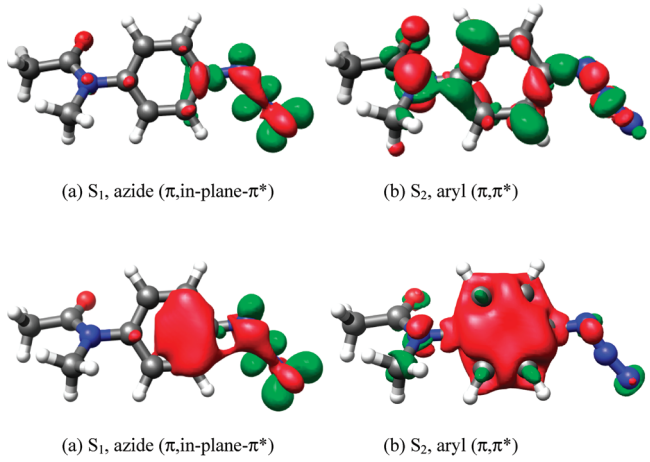

Figure 2. Difference density plots for 4-*N*-methylacetamidophenyl azide (**1b**) at the TD-B3LYP/TZVP, (a) S_1 and (b) S_2, and at the RI-CC2/TZVP, (c) S_1 and (d) S_2, levels of theory. (The green contours depict the accumulation of electron density in the excited state, and the red contours illustrate the loss of electron density from the S_0 ground state. The isocontour values are adjusted differently for appropriate visualization: TD-B3LYP, S_1 ±0.005, S_2 ±0.002; RI-CC2, S_1 −0.02, +0.005, S_2 −0.01, +0.0005 au.)

obtain the electron density changes for the different excited states. Furthermore, to gain insight into the character of the nitrenes, we performed CASSCF calculations for both open-shell and closed-shell descriptions of the singlet phenylnitrenes with the Gaussian 03 program[72] and CASPT2 energy corrections with MOLCAS 7.4 program.[73] All of these excited-state calculations and CASSCF analyses were performed at the Ohio Supercomputer Center.

RESULTS AND DISCUSSION

A. Excited State Calculations on Azide Singlet Surfaces. All of these calculations were performed with C_1 symmetry. The 4-*N*-methylacetamidophenyl azide has a 50° torsion angle between the substituent and the phenyl ring, whereas the 4-acetamidophenyl azide is almost planar in the ground state (See Supporting Information.) Calculated ground-state absorption features for both of the azides are tabulated in Table 1. For both azides, the transition to the lowest singlet excited state is calculated to be very weak as the oscillator strength is less than 10^{-3}. On the other hand, the second excited state is calculated to have about 50−1000 times higher oscillator strength; therefore, we speculate that the azides are initially excited to the S_2 surface when photoexcited by 266 nm light. The comparison between the calculated and experimental spectra is represented in Figure 1S in Supporting Information.

To gain insight into the character of these singlet excited states, we computed the electronic difference densities between the ground and excited state wave functions. These difference density plots are useful in the cases of multiconfigurational vertical excitations, for which the inspection of individual orbitals may not be as useful. We have recently utilized this strategy in many different photochemical problems.[74] Subtraction of the ground-state electron density from the Franck−Condon, excited-state electron density yields a difference density plot which reveals the movement of electron density upon excitation. A green color shows the accumulation of electron density in the Franck−Condon excited state, while a red color indicates the loss of electron density from the ground state. Difference density plots for both the S_1 and S_2 excited states are shown in Figure 1 for 4-acetamidophenyl azide (**1a**) and in Figure 2, for 4-*N*-methylacetamidophenyl azide (**1b**) at both RI-CC2/TZVP and TD-B3LYP/TZVP level of theories.

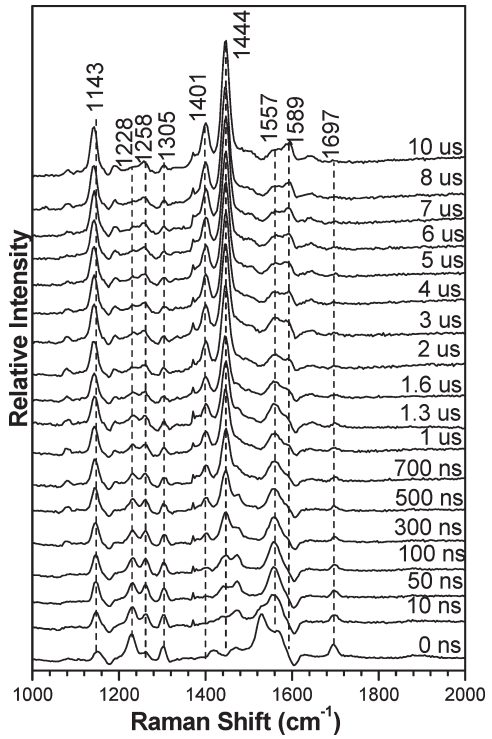

Figure 3. Overview of 319.9 nm probe TR^3 spectra obtained after 266 nm photolysis of 2 mM 4-acetamidophenyl azide in acetonitrile under air. The time delays between the pump (266 nm) and probe (319.9 nm) laser beams are shown to the right of each spectrum, and the Raman shifts of selected bands are presented at the top of the 10 μs spectrum. See text for more details.

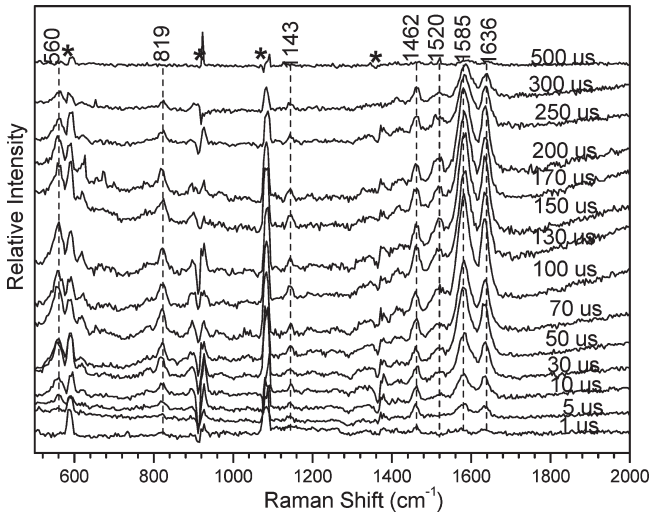

Figure 4. 319.9 nm probe TR^3 spectra obtained after 266 nm photolysis of 2 mM 4-*N*-methylacetamidophenyl azide in acetonitrile. The time delays between the pump (266 nm) and probe (319.9 nm) laser beams are shown to the right of each spectrum, and the Raman shifts of selected bands are presented at the top of the 500 μs spectrum. See text for more details.

The difference density plots are quite similar for azides **1a** and **1b**, and both of the theoretical methods are in good agreement with each other. The plots corresponding to the S_1 surface suggest that the lowest singlet excited state is localized mainly on the azide unit. The electron density is depleted from the π-orbital of the azide and is transferred to the in-plane π^* orbital of the azide. The difference density changes indicate that the $ArN-N_2$ bond will lengthen on the S_1 surface, followed by formation of the singlet nitrene and molecular nitrogen. Similar difference density plots were reported earlier by us for different aryl azides[74] and are characteristic of the azide dissociative states. On the other hand, for the S_2 state, the electron density movement is localized on the phenyl ring, which indicates that this excitation is a (π,π^*) excited state on the aromatic unit. This is also supported by the observation that the S_2 state has a much higher oscillator strength compared to the S_1 state (Table 1). Overall, these difference density plots suggest that irradiation of 4-acetamidophenyl and 4-*N*-methylacetamidophenyl azides with 266 nm light should excite each system to the S_2 state which is phenyl (π,π^*) in character, with subsequent relaxation to the S_1 surface which is the azide dissociative state, thereby forming the substituted phenylnitrene.

B. Time-Resolved Resonance Raman (TR^3) Spectra Acquired after 266 nm Photolysis of 4-Acetamidophenyl Azide and 4-*N*-Methylacetamidophenyl Azide in Acetonitrile. Figure 3 displays TR^3 spectra acquired at various time delays after photolysis of 2 mM 4-acetamidophenyl azide in acetonitrile. The time delays between the pump (266 nm) and probe (319.9 nm) laser pulses are shown to the right of each spectrum, and the Raman shifts of selected bands are presented at the top of the 10 μs spectrum. Inspection of Figure 3 shows there are three species observed on the 0 ns to 10 μs time scale. The first species has characteristic Raman bands at 1224, 1419, 1528, and 1693 cm^{-1} and appears to decay completely within 50 ns to form a second species. The second species has characteristic Raman bands at 1258 and 1557 cm^{-1} and decays to produce a third species with characteristic Raman bands at 1401 and 1444 cm^{-1}. Similar TR^3 experiments were also performed under oxygen purging conditions, and the resulting transient spectra are shown in Figure 2S (Supporting Information). Close examination of the TR^3 spectra shows that the presence of oxygen reduces the yield of the third species, as under identical experimental conditions, the yield of the third species obtained with oxygen purging is only 80% of that obtained under air. We propose that the third species in the TR^3 spectra in Figure 3 be assigned to an azo compound formed from the triplet nitrene and that the second species is the triplet nitrene.

Figure 4 displays TR^3 spectra acquired at various time delays after 266 nm photolysis of 2 mM 4-*N*-methylacetamidophenyl azide in acetonitrile. The time delays between the pump (266 nm) and probe (319.9 nm) laser pulses are shown to the right of each spectrum, and the Raman shifts of selected bands are presented at the top of the spectrum recorded 500 μs after the laser pulse. Inspection of Figure 4 shows that only one species can be observed between 0 ns and 500 μs. This species forms on the time scale of about several tens of microseconds, which is much slower than the formation of the third species observed in the TR^3 spectra of Figure 3. Moreover, the species observed in Figure 4 has the strongest Raman band at 1585 cm^{-1} and the second most intense Raman band at 1636 cm^{-1}. This is significantly different from the Raman spectra in Figure 3 that have their most intense Raman bands in the 1400−1500 cm^{-1} region. These significant differences in the Raman spectra and the formation rates between the species observed in Figures 3 and 4 indicate that the species in Figure 4 obtained from photolysis of 4-*N*-methylacetamidophenyl azide in acetonitrile

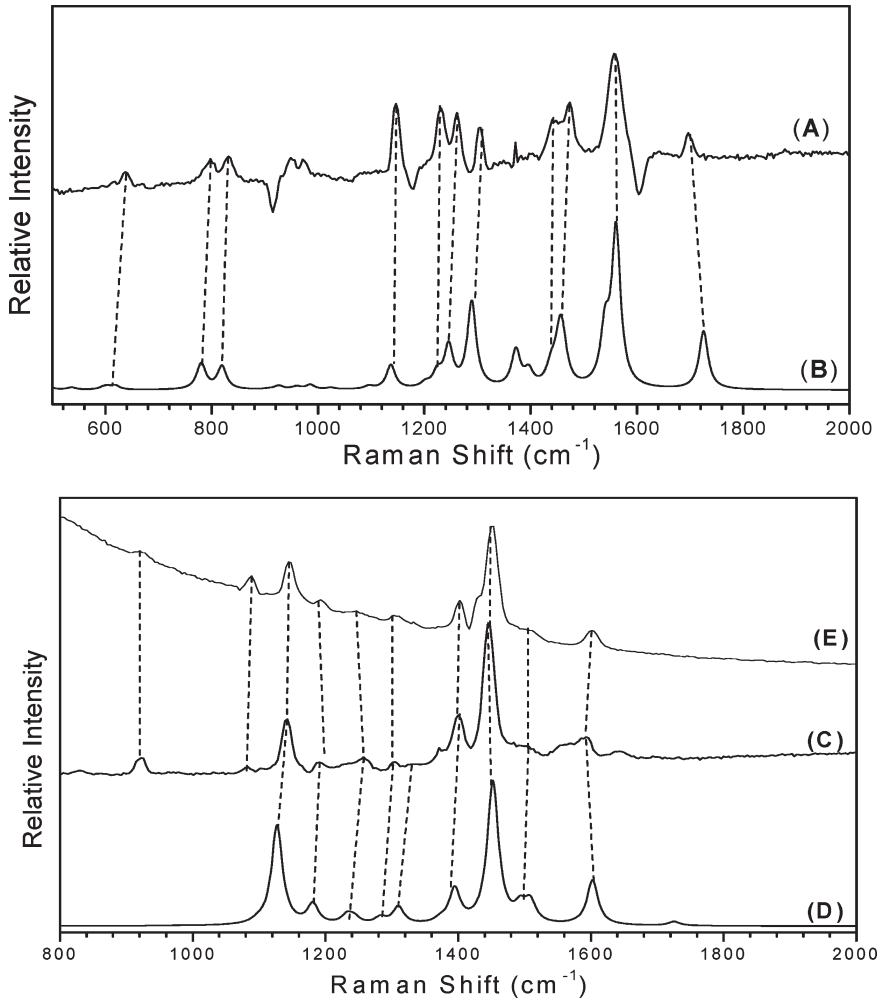

Figure 5. Comparison of (A) the experimental 50 ns and (C) 10 μs TR^3 spectra from Figure 3 to the UB3LYP/6-31G* calculated normal Raman spectrum for (B) triplet 4-acetamidophenylnitrene and (D) 4,4′-bisacetamidoazobenzene and (E) 319.9 nm pumped resonance Raman spectrum of synthesized authentic 4,4′-bisacetamidoazobenzene. The calculated relative Raman intensities were convoluted with a Lorentzian function. See text and Tables 1S and 2S (Supporting Information) for more details.

has a very different structure from the species observed in Figure 3 obtained from photolysis of 4-acetamidophenyl azide and therefore cannot be an azo compound. Consequently, singlet 4-*N*-methylacetamidophenylnitrene does not relax to its lower energy triplet state but mostly undergoes the ring expansion rearrangement pathway instead.

C. Assignments of the Species Observed in the TR^3 Spectra. Comparison of experimental vibrational frequencies to those predicted from density functional theory (DFT) or ab initio calculations for probable intermediates has been successfully employed to identify and assign time-resolved infrared (TR-IR) and time-resolved resonance Raman (TR^3) spectra to arylnitrenium ions, arylnitrenes, and arylnitrene photoproducts.[48,56,57b,60,63−65] We shall use similar methodology to help assign the four species observed in the TR^3 spectra of Figures 3 and 4. DFT calculations were performed to test these possibilities. (U)B3LYP/6-31G* calculations were used to predict the total energy, the optimized geometry, and vibrational frequencies for the triplet 4-acetamidophenylnitrene and the azo compound, 4,4′-bisacetamidoazobenzene. Figure 5 compares the experimental 50 ns and 10 μs TR^3 spectra, post laser pulse, from Figure 3 to the (U)B3LYP/6-31G* calculated normal Raman spectra whose relative intensities were convoluted with a Lorentzian function. Inspection of Figure 5 shows that the experimental 50 ns and 10 μs TR^3 spectra (spectra A and C) agree well with the calculated normal Raman spectra for the triplet 4-acetamidophenylnitrene species and the 4,4′-bisacetamidoazobene product (spectra B and D), respectively, with some moderate differences in the relative intensities that can be easily accounted for by the fact that the experimental spectra are resonantly enhanced while the calculated spectra are for normal (nonresonance) Raman spectra. Tables 1S and 2S of the Supporting Information compare the experimental and the calculated Raman band vibrational frequencies for the species shown in Figure 5 and the differences between the experimental and calculated frequencies are, on average, only 11.8 cm^{-1} for the triplet 4-acetamidophenylnitrene and 9.1 cm^{-1} for the 4,4′-bisacetamidoazobene. All of these results indicate that the second and the third species observed in Figure 3 are the triplet 4-acetamidophenylnitrene and the azo compound, 4,4′-bisacetamidoazobene, respectively. In order to unequivocally confirm the assignment of the third species, the authentic 4,4′-bisacetamidoazobenzene compound was synthesized and we compared its 319.9 nm pumped resonance Raman spectrum (spectrum E) to the experimental 10 μs postpulse TR^3 spectra as shown in

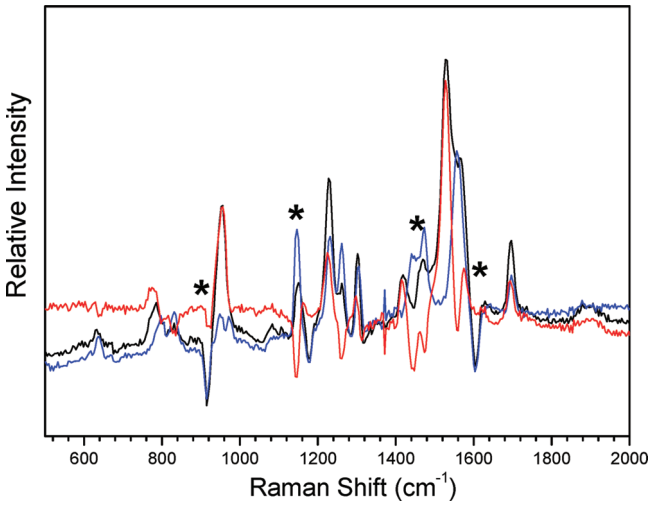

Figure 6. Raman spectrum of singlet 4-acetamidophenylnitrene (red) obtained by subtraction of a scaled Raman spectrum of triplet nitrene (blue) from the TR^3 spectrum (black) obtained at 0 ns, in Figure 3. Star symbols mark solvent-subtraction artifacts and stray-light and ambient-light artifacts.

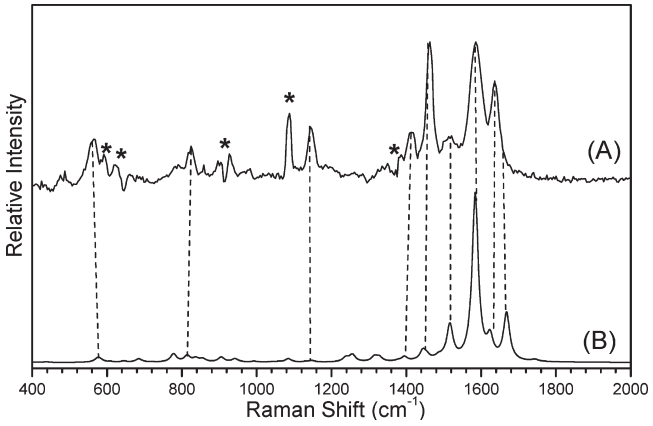

Figure 7. Comparison of (A) the 100 μs experimental TR^3 spectrum in Figure 4 to (B) the B3LYP/6-31G* calculated normal Raman spectrum for the dimer formed from 1,2-didehydroazepines. The calculated relative Raman intensities were convoluted with a Lorentzian function. See text for more details.

Figure 5. These two spectra (spectra C and E) are essentially identical within experimental uncertainty, and this unambiguously confirms the assignment of the third species to the azo type compound.

The first species in Figure 3 was observed at 0 and 10 ns time delays and decayed completely within 50 ns to form the triplet 4-acetamidophenylnitrene. The singlet 4-acetamidophenylnitrene was found to have a sufficiently long lifetime to be trapped by water to produce the corresponding arylnitrenium ion[63] Furthermore, a singlet aryl azide excited state typically has a lifetime of only 150−300 fs; thus this experimentally observed species is not a singlet azide excited state, but the singlet nitrene. The Raman spectrum of the singlet 4-acetamidophenylnitrene, alone, is presented in Figure 6. It was obtained by subtraction of an appropriately scaled triplet 4-acetamidophenylnitrene spectrum (50 ns TR^3 spectrum) from the TR^3 spectrum obtained at 0 ns in Figure 3.

Resonance Raman spectra have been obtained for a number of azo compounds, and these resonance Raman spectra typically have most of their intensity in Raman bands associated with the N═N chromophore and corresponding vibrational modes in the ν = 1400−1500 cm^{-1} region with moderate intensity in bands above 1500 cm^{-1} associated with aromatic C═C bonds,[64a,65e,75] which are in agreement with the 10 μs TR^3 spectrum in Figure 3. But the species observed in Figure 4 has most of its Raman intensity at about 1600 cm^{-1} associated with the C═C stretch vibrational modes, and only moderate intensity in the 1400−1500 cm^{-1} region. Hypothetically, the Raman spectrum of the 4-*N*-methylacetamido substituted azo compound should be similar to that of the 4-acetamido substituted azo compound because of the great similarity in their structure, but this is not the experimental result. Thus, it is unlikely that the species observed in Figure 4 is that of an azo compound with an N═N chromophore. Instead, the species may be eventually produced from the ring expansion rearrangement reaction. Another class of species with dimeric structures was found upon photolysis of phenyl azide, 3-hydroxyphenyl azide, and 3-methoxyphenyl azide in room temperature solutions. These dimers were believed to form by dimerization of 1,2-didehydroazepine and were characterized using Raman spectroscopy. The Raman spectra in Figure 4 are very similar to those of dimers formed from 1,2-didehydroazepines in terms of both their Raman band patterns and formation rate. Consequently, this kind of dimer with 4-*N*-methylacetamido substitution was considered with DFT calculations. The comparison of the experimental Raman spectrum of Figure 4 to the calculated normal Raman spectrum of a dimer formed from 1,2-didehydroazepines is displayed in Figure 7 and comparisons of some specific vibrational frequencies are listed in Table 3S (Supporting Information). Examination of Figure 7 and Table 3S (Supporting Information) shows that there is reasonable agreement between the computational and experiment results considering the differences associated with normal and resonance Raman in regard to their relative intensities. These results indicate that the species observed in Figure 4 obtained after photolysis of 4-*N*-methylacetamidophenyl azide in acetonitrile is the dimer formed from dimerization of 4-*N*-methylacetamido substituted 1,2-didehydroazepines. The didehydroazepine **6b** was not observed during TR^3 experiments even though it is well-known that a didehydroazepine has a strong characteristic IR band at ∼1880 cm^{-1}. However the DFT calculation predicts that **6b** has an IR intensity of 164 Km/mol for the C═C═N vibration mode while the Raman activity is only 12 Å^4/amu. This is due to different selection rules for Raman scattering and infrared absorbance. It also accounts for the failure to observe the didehydroazepine in TR^3 experiments.

D. Discussion of the 4-Acetamido and 4-*N*-Methylacetamido Substitution Influence on ISC Rate of Singlet Phenylnitrenes. Parent phenylnitrene has a relatively slow ISC rate with a time constant of $(3.2 \pm 0.3) \times 10^6$ s^{-1} because singlet phenylnitrene is an open-shell singlet species for which the effective intersystem crossing mechanism, spin−orbit coupling, is forbidden and thus ineffective in promoting ISC.[69] Electron-donating groups have been observed to greatly influence ISC rates. *p*-Methoxy and dimethylamino substituents were observed to accelerate the ISC rates with observed time constants of about $>5 \times 10^8$ s^{-1} for *p*-methoxy[54] and $(8.3 \pm 0.2) \times 10^9$ s^{-1} for *p*-dimethylamino[69] phenylnitrene. Triplet 4-biphenylylnitrene and its corresponding azo compound dimer were also observed by TR^3 spectroscopy.[64a] All of these singlet phenylnitrenes have

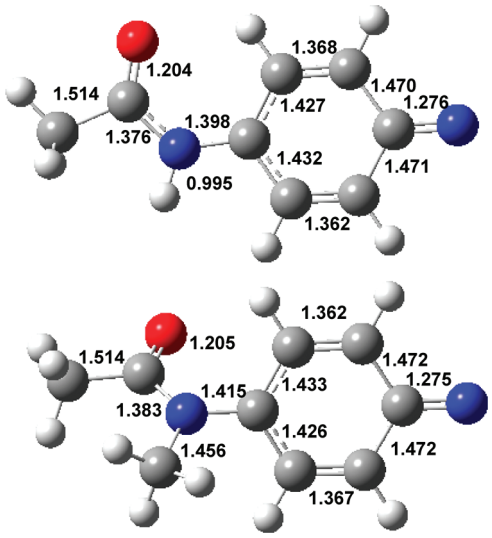

Figure 8. Optimized geometries of 4-acetamido (top) and 4-*N*-methylacetamido phenylnitrene (bottom) in open-shell electronic configuration at the CASSCF(12,11)/6-31G* level of theory.

ionic character, which can increase the spin-obit coupling and the rate constant of intersystem crossing. The ring-expansion pathways that form 1,2-didehydroazepines are sensitive to substitution, in the case of the strongest para donor, MeNH−, this barrier increased to about 13 kcal·mol^{-1},[76] as compared to ∼6 kcal·mol^{-1} for singlet phenylnitrene.

In order to characterize the electronic structure of the nitrenes generated, we performed CASSCF calculations to assess the open-shell or closed-shell nature of these singlet intermediates. Ideally, all of the π-orbitals and π-electrons must be used to perform accurate CASSCF calculations, i.e., 14 electrons in 12 orbitals in these cases. However, attempts to optimize the closed-shell configurations with the ideal active space for 4-acetamidophenylnitrene and 4-*N*-methylacetamidophenylnitrene yielded an open-shell electronic configuration. Furthermore, we tried to optimize both open-shell and closed-shell configurations with reduced active spaces. In the case of 4-acetamidophenylnitrene, we were able to optimize both configurations at the CASSCF(8,7), CASSCF(6,5), and CASSCF(4,3) levels with the 6-31G* basis set. These calculations revealed the energy difference between the two configurations of 13.4, 24.2, and 5.3 kcal·mol^{-1} making the open-shell electronic configuration the preferred description of the singlet state of both nitrenes. The inconsistency in the energy gap is probably due to the lack of certain π-orbitals in the active space. However, in all of these cases, the open-shell configuration is consistently the preferred description. Furthermore, attempts to optimize the closed-shell configuration for the 4-*N*-methylacetamidophenylnitrene with reduced active spaces also converged on the open-shell solution. This CASSCF analysis predicts that both nitrenes are open shell in their lowest energy singlet state; however, we were not able to obtain the exact energy difference between the two electronic structures of the singlet nitrenes. To calculate the energy gaps between the closed-shell and open-shell configurations of the two singlet nitrenes, we performed CASSCF(12,11)/6-31G* calculations. A second-order perturbation level correction (CASPT2) was made to the CASSCF(12,11)/6-31G* wave function using the same active space and basis set. These calculations revealed that both singlet 4-acetamido and 4-*N*-methylacetamidophenylnitrenes preferred to be open shell in their lowest singlet state and the corresponding closed-shell analogues are 19.3 and 20.4 kcal/mol above the open-shell description, respectively.

The 4-acetamido and 4-*N*-methylacetamido groups are both electron-donating groups; however, the two substituted singlet phenylnitrenes have quite different geometries. Figure 8 shows optimized geometries of singlet 4-acetamido and 4-*N*-methylacetamido phenylnitrenes in their open-shell electronic configurations at the CASSCF(12,11) level of theory. (See Supporting Information for optimized geometries at other active spaces.) The C−N bond lengths at the nitrene end of the molecules are ca. 1.276 Å, which suggest similar communication between the nitrene orbitals and the aromatic π-system for both of the molecules. Conversely, the geometry at the substituent end is quite different in these two nitrene species. The C−N-(X)COCH$_3$ bond is lengthened in the case of 4-*N*-methylacetamido phenylnitrene. Furthermore, the substituent, 4-*N*-methylacetamido group is also significantly out-of-plane (ca. 45−55°) with respect to the aromatic system while the 4-acetamido group is almost planar (ca. 0−1°). These factors might play an important role in understanding the experimentally observed different photochemical behavior of these singlet phenylnitrenes.

In our TR^3 experiments, the triplet 4-acetamidophenylnitrene and its corresponding azo compound were observed, consistent with the expectation that strongly electron-donating groups accelerate the ISC rate. In contrast, it is neither the triplet nitrene nor an azo compound, but the ring expansion product instead, the dimer formed from 1,2-didehydroazepines that was observed in the TR^3 spectra after photolysis of 4-*N*-methylacetamidophenyl azide in acetonitrile. Evidently, the 4-acetamido substitution has a substantial influence on the ISC transition rate of singlet phenylnitrene but the 4-*N*-methylacetamido group does not. In order to provide an explanation to this photochemical disparity, we evaluated the singlet−triplet energy gap for these substituted nitrenes. Thus, we optimized the triplet nitrenes at the CASSCF-(12,11)/6-31G* level of theory, and the optimized triplet states were found to have their unpaired electrons localized on the nitrogen of the substituted phenylnitrene. The difference between the open-shell singlet and the triplet nitrene is estimated to be about 16.9 and 16.8 kcal·mol^{-1} for 4-acetamidophenylnitrene and 4-*N*-methylacetamidophenylnitrene, respectively, with the triplet as the energetically favored state in each case. This suggests that the energetic separation between the singlet and triplet states is not a significant factor in the divergence in the photochemistry. However, the optimized geometries of these singlet and triplet nitrenes provided an insight as to why 4-*N*-methylacetamidophenylnitrene does not follow the expected mechanism. The 4-acetamidophenylnitrene remained to be planar in singlet as well as triplet manifolds allowing interaction of the lone pair of electrons on nitrogen with the aromatic ring and the nitrene nitrogen. It is well-known that *p*-methoxy and dimethylamino substituents accelerate ISC relative to parent phenylnitrene.[54,69] This has been attributed to the stabilization of ionic resonance structures that are essential to spin−orbit coupling.[78]

However, both the singlet and triplet 4-*N*-methylacetamido phenylnitrene have the *N*-methylacetamido substituent about 50° out-of-plane relative to the plane of the aromatic unit, thereby disrupting overlap between orbitals of the electron-donating acetamide nitrogen and the aromatic π system. Consequently, there is a diminished contribution of the electron-donating

qeffect by the *N*-methylacetamido substituent, less spin−orbit coupling and reduced acceleration of ISC. Thus singlet nitrene isomerization to form 1,2-didehydroazepines is now faster than ISC to the triplet.

CONCLUSIONS

Time-resolved resonance Raman investigations of the photochemistry of 4-acetamidophenyl azide and 4-*N*-methylacetamidophenyl azide are reported. Computational study of the excited states suggests excitation to the S_2 surface, followed by fast internal conversion and formation of arylnitrene on the S_1 surface. Photolysis of 4-acetamidophenyl azide in acetonitrile at 266 nm showed the signatures of three species in TR^3 spectra within 10 μs after excitation. These three species were assigned to be the singlet and triplet 4-acetamidophenylnitrenes and 4,4′-bisacetamidoazobenzene, respectively. In contrast, only one species was observed in the TR^3 spectra after photolysis of 4-*N*-methylacetamidophenyl azide in acetonitrile, and was tentatively assigned to the ring-expansion product, the dimer which is formed from dimerization of a 1,2-didehydroazepine. These different reaction pathways of two 4-acetamido substituted singlet phenylnitrenes demonstrate that the 4-acetamido substitution on phenylnitrene must have a substantial influence on the ISC rate of the singlet phenylnitrene, but the 4-*N*-methylacetamido group does not. The CASSCF calculations suggested that both of the nitrenes are open shell in character for the singlet state, and furthermore, the singlet−triplet energy gap is also very similar for both nitrenes. However, the differences in the photochemical mechanism are interpreted due to a nullified electron-donating effect of the 4-*N*-methylacetamido substituent because of the distortion of this substituent (∼50°) relative to the phenyl plane, while the 4-acetamido group was almost planar. This twisting of the 4-*N*-methylacetamido substituent renders limited conjugation between the substituent and the nitrene center and dramatically alters the ISC rate, thus leading to different photochemical consequences relative to the 4-acetamido substituted case.

ASSOCIATED CONTENT

Supporting Information. Figure 1S shows a comparison between the calculated ground state azides absorption and the experimental UV−vis spectra, Figure 2S shows an overview of the 319.9 nm probe TR^3 spectra obtained after 266 nm photolysis of 2 mM 4-acetamidophenyl azide in acetonitrile (under O_2 purge conditions), Table 1S shows a comparison of the calculated Raman vibrational frequencies for the triplet 4-acetamidophenylnitrene to those observed for the 50 ns TR^3 experimental spectrum of Figure 3, Table 2S shows comparison of calculated Raman vibrational frequencies for the 4,4′-bisacetamidoazobene compound to those observed for the 10 μs TR^3 experimental spectrum of Figure 3, Table 3S shows comparison of calculated Raman vibrational frequencies for the dimer formed from 1,2-didehydroazepines to those observed for the 100 μs TR^3 experimental spectrum of Figure 4, Cartesian coordinates, total energies, and vibrational zero-point energies for the optimized geometry from the B3LYP/6-31G* calculations for the triplet 4-acetamidophenylnitrene, 4,4′-bisacetamidoazobene, and 4-*N*-methylacetamido substituted dimer formed from 1,2-didehydroazepine. This material is available free of charge via the Internet at http://pubs.acs.org.

AUTHOR INFORMATION

Corresponding Author

*E-mail: phillips@hkucc.hku.hk; hadad.1@osu.edu; platz.1@osu.edu.

ACKNOWLEDGMENT

This work was supported by grants from the Research Grants Council (RGC) of Hong Kong (HKU-7039/07P) to D.L.P., while C.M.H. and M.S.P. acknowledge financial support of this work by the US National Science Foundation (CHE-0743258). Generous computational resourced from the Ohio Supercomputer Center is also gratefully acknowledged. S.V. acknowledges the OSU University Presidential Fellowship.

REFERENCES

(1) (a) Smith, P. A. S. In *Nitrenes*; Lwowski, W., Ed.; Wiley-Interscience: New York, 1970; Chapter 4. (b) Scriven, E. F. V. In *Reactive Intermediates*; Abramovich, R. A., Ed.; Plenum: New York, 1982; Vol. 2, Chapter 1.

(2) C. Wentrup, C. *Reactive Molecules*; Wiley-Interscience: New York, 1984; Chapter 4.

(3) Platz, M. S. In *Azides and Nitrenes: Reactivity and Utility*; Scriven, E. F. V., Ed.; Academic: New York, 1984; Chapter 7.

(4) Platz, M. S.; Maloney, V. M. In *Kinetics and Spectroscopy of Carbenes and Biradicals*; Platz, M. S., Ed.; Plenum: New York, 1990; pp 303−320.

(5) Platz, M. S.; Leyva, E.; Haider, K. *Org. Photochem.* **1991**, *11*, 367–398.

(6) Schuster, G. B.; Platz, M. S. *Adv. Photochem.* **1992**, *17*, 69–143.

(7) Platz, M. S. *Acc. Chem. Res.* **1995**, *28*, 487–492.

(8) Borden, W. T.; Gritsan, N. P.; Hadad, C. M.; Karney, W. L.; Kemnitz, C. R.; Platz, M. S. *Acc. Chem. Res.* **2000**, *33*, 765–771.

(9) Schrock, A. K.; Schuster, G. B. *J. Am. Chem. Soc.* **1984**, *106*, 5228–5234.

(10) Donnelly, T.; Dunkin, I. R.; Norwood, D. S. D.; Prentice, A.; Shields, C. J.; Thomson, P. C. P. *J. Chem. Soc., Perkin Trans. 2* **1985**, 307–310.

(11) Dunkin, I. R.; Donnelly, T.; Lockhart, T. S. *Tetrahedron Lett.* **1985**, *26*, 359–362.

(12) Leyva, E.; Platz, M. S. *Tetrahedron Lett.* **1985**, *26*, 2147–2150.

(13) Leyva, E.; Platz, M. S.; Persy, G.; Wirz, J. *J. Am. Chem. Soc.* **1986**, *108*, 3783–3790.

(14) Shields, C. J.; Chrisope, D. R.; Schuster, G. B.; Dixon, A. J.; Poliakoff, M.; Turner, J. J. *J. Am. Chem. Soc.* **1987**, *109*, 4723–4726.

(15) Li, Y.-Z.; Kirby, J. P.; George, M. W.; Poliakoff, M.; Schuster, G. B. *J. Am. Chem. Soc.* **1988**, *110*, 8092–8098.

(16) Poe, R.; Grayzar, J.; Young, M. J. T.; Leyva, E.; Schnapp, K.; Platz, M. S. *J. Am. Chem. Soc.* **1991**, *113*, 3209–3211.

(17) Young, M. J. T.; Platz, M. S. *J. Org. Chem.* **1991**, *56*, 6403–6406.

(18) Poe, R.; Schnapp, K.; Young, M. J. T.; Grayzar, J.; Platz, M. S. *J. Am. Chem. Soc.* **1992**, *114*, 5054–5067.

(19) Younger, C. G.; Bell, R. A. *J. Chem. Soc., Chem. Commun.* **1992**, 1359–1361.

(20) Kim, S.-J.; Hamilton, T. P.; Schaefer, H. F. *J. Am. Chem. Soc.* **1992**, *114*, 5349–5355.

(21) Hrovat, D. A.; Waali, E. E.; Borden, W. T. *J. Am. Chem. Soc.* **1992**, *114*, 8698–8699.

(22) Marcinek, A.; Platz, M. S. *J. Phys. Chem.* **1993**, *97*, 12674–12677.

(23) Marcinek, A.; Leyva, E.; Whitt, D.; Platz, M. S. *J. Am. Chem. Soc.* **1993**, *115*, 8609–8612.

(24) Schnapp, K. A.; Poe, R.; Leyva, E.; Soundarajan, N.; Platz, M. S. *Bioconjugate Chem.* **1993**, *4*, 172–177.

(25) Schnapp, K. A.; Platz, M. S. *Bioconjugate Chem.* **1993**, *4*, 178–183.
(26) Anderson, G. B.; Falvey, D. E. *J. Am. Chem. Soc.* **1993**, *115*, 9870–9871.
(27) Ohana, T; Kaise, M.; Nimura, S.; Kikuchi, O.; Yabe, A. *Chem. Lett.* **1993**, 765–768.
(28) Davidse, P. A.; Kahley, M. J.; McClelland, R. A.; Novak, M. *J. Am. Chem. Soc.* **1994**, *116*, 4513–4514.
(29) Marcinek, A.; Platz, M. S.; Chan, Y. S.; Floresca, R.; Rajagopalan, K.; Golinski, M.; Watt, D. *J. Phys. Chem.* **1994**, *98*, 412–419.
(30) Lamara, K.; Redhouse, A. D.; Smalley, R. K.; Thompson, J. R. *Tetrahedron* **1994**, *50*, 5515–5526.
(31) McClelland, R. A.; Davidse, P. A.; Haczialic, G. *J. Am. Chem. Soc.* **1995**, *117*, 4173–4174.
(32) Robbins, R. J.; Yang, L. L.-N.; Anderson, G. B.; Falvey, D. E. *J. Am. Chem. Soc.* **1995**, *117*, 6544–6552.
(33) Srivastava, S.; Falvey, D. E. *J. Am. Chem. Soc.* **1995**, *117*, 10186–10193.
(34) McClelland, R. A.; Kahley, M. J.; Davidse, P. A. *J. Phys. Org. Chem.* **1996**, *9*, 355–360.
(35) McClelland, R. A.; Kahley, M. J.; Davidse, P. A.; Hadzialic, G. *J. Am. Chem. Soc.* **1996**, *118*, 4794–4803.
(36) Robbins, R. J.; Laman, D. M.; Falvey, D. E. *J. Am. Chem. Soc.* **1996**, *118*, 8127–8135.
(37) Moran, R. J.; Falvey, D. E. *J. Am. Chem. Soc.* **1996**, *118*, 8965–8966.
(38) Morawietz, J.; Sander, W. *J. Org. Chem.* **1996**, *61*, 4351–4354.
(39) Castell, O.; Garcia, V. M.; Bo, C.; Caballol, R. *J. Comput. Chem.* **1996**, *17*, 42–48.
(40) Michalak, J.; Zhai, H. B.; Platz, M. S. *J. Phys. Chem.* **1996**, *100*, 14028–14036.
(41) Sun, X.-Z.; Virrels, I. G.; George, M. W.; Tomioka, H. *Chem. Lett.* **1996**, 1089–1090.
(42) Karney, W. L.; Borden, W. T. *J. Am. Chem. Soc.* **1997**, *119*, 1378–1387.
(43) Karney, W. L.; Borden, W. T. *J. Am. Chem. Soc.* **1997**, *119*, 3347–3350.
(44) Gritsan, N. P.; Yuzawa, T.; Platz, M. S. *J. Am. Chem. Soc.* **1997**, *119*, 5059–5060.
(45) Born, R.; Burda, C.; Senn, P.; Wirz, J. *J. Am. Chem. Soc.* **1997**, *119*, 5061–5062.
(46) Gritsan, N. P.; Zhai, H. B.; Yuzawa, T.; Karweik, D.; Brooke, J.; Platz, M. S. *J. Phys. Chem. A* **1997**, *101*, 2833–2840.
(47) Moran, R. J.; Falvey, D. E. *J. Am. Chem. Soc.* **1996**, *118*, 8965–8966.
(48) Srivastava, S.; Toscano, J. P.; Moran, R. J.; Falvey, D. E. *J. Am. Chem. Soc.* **1997**, *119*, 11552–11553.
(49) Leyva, E.; Sagredo, R. *Tetrahedron* **1998**, *54*, 7367–7374.
(50) Nicolaides, A.; Tomioka, H.; Murata, S. *J. Am. Chem. Soc.* **1998**, *120*, 11530–11531.
(51) Nicolaides, A.; Nakayama, T.; Yamazaki, K.; Tomioka, H.; Koseki, S.; Stracener, L. L.; McMahon, R. J. *J. Am. Chem. Soc.* **1999**, *121*, 10563–10572.
(52) Gritsan, N. P.; Zhu, Z.; Hadad, C. M.; Platz, M. S. *J. Am. Chem. Soc.* **1999**, *121*, 1202–1207.
(53) Gritsan, N. P.; Gudmundsdottir, A. D.; Tigelaar, D.; Platz, M. S. *J. Phys. Chem. A* **1999**, *103*, 3458–3461.
(54) Gritsan, N. P.; Tigelaar, D.; Platz, M. S. *J. Phys. Chem. A* **1999**, *103*, 4465–4469.
(55) Cerro-Lopez, M.; Gritsan, N. P.; Zhu, Z.; Platz, M. S. *J. Phys. Chem. A* **2000**, *104*, 9681–9686.
(56) Srivastava, S.; Ruane, P. H.; Toscano, J. P.; Sullivan, M. B.; Cramer, C. J.; Chiapperino, D.; Reed, E. C.; Falvey, D. E. *J. Am. Chem. Soc.* **2000**, *122*, 8271–8278.
(57) (a) Gritsan, N. P.; Likhotvorik, I.; Tsao, M.-L.; Celebi, N.; Platz, M. S.; Karney, W. L.; Kemnitz, C. R.; Borden, W. T. *J. Am. Chem. Soc.* **2001**, *123*, 1425–1433. (b) Tsao, M.-L.; Gritsan, N.; James, T. R.; Platz, M. S.; Hrovat, D. A.; Borden, W. T. *J. Am. Chem. Soc.* **2003**, *125*, 9343–9358.
(58) Inui, H.; Murata, S. *Chem. Lett.* **2001**, 832–833.
(59) Nicolaides, A.; Enyo, T.; Miura, D.; Tomioka, H. *J. Am. Chem. Soc.* **2001**, *123*, 2628–2636.
(60) (a) Ong, S. Y.; Zhu, P.; Poon, Y. F.; Leung, K.-H.; Fang, W. H.; Phillips, D. L. *Chem.—Eur. J.* **2002**, *8*, 2163–2171. (b) Ong, S. Y.; Zhu, P.; Leung, K. H.; Phillips, D. L. *Chem.—Eur. J.* **2003**, *9*, 1377–1386. (c) Ong, S. Y.; Chan, P. Y.; Zhu, P.; Leung, K. H.; Phillips, D. L. *J. Phys. Chem. A* **2003**, *107*, 3858–3865.
(61) Miura, A.; Kobayashi, T. *J. Photochem. Photobiol., A* **1990**, *53*, 223.
(62) (a) Ruane, P. H.; McClelland, R. A. *Can. J. Chem.* **2001**, *79*, 1875–1880. (b) Brown, B. R.; Yielding, L. W.; White, W. E. *Mutat. Res.* **1980**, *70*, 17–27. (c) Wheeler, O. H.; Gonzalez, D. *Tetrahedron* **1964**, *20*, 189–193.
(63) Chan, P. Y.; Ong, S. Y.; Zhu, P.; Leung, K. H.; Phillips, D. L. *J. Org. Chem.* **2003**, *68*, 5265–5273.
(64) (a) Chan, P. Y.; Ong, S. Y.; But, T. Y. S.; Phillips, D. L. *J. Raman Spectrosc.* **2004**, *35*, 887–894. (b) Kwok, W. M.; Chan, P. Y.; Phillips, D. L. *J. Phys. Chem. B* **2004**, *108*, 19068–19075.
(65) (a) Zhu, P.; Ong, S. Y.; Chan, P. Y.; Leung, K. H.; Phillips, D. L. *J. Am. Chem. Soc.* **2001**, *123*, 2645–2649. (b) Zhu, P.; Ong, S. Y.; Chan, P. Y.; Poon, Y. F.; Leung, K. H.; Phillips, D. L. *Chem.—Eur. J.* **2001**, *7*, 4928–4936. (c) Chan, P. Y.; Ong, S. Y.; Zhu, P.; Zhao, C.; Phillips, D. L. *J. Phys. Chem. A* **2003**, *107*, 8067–8074. (d) Chan, P. Y.; Kwok, W. M.; Lam, S. K.; Chiu, P.; Phillips, D. L. *J. Am. Chem. Soc.* **2005**, *127*, 8246–8247. (e) Xue, J.; Guo, Z.; Chan, P. Y.; Chu, L. M.; But, T. Y. S.; Phillips, D. L. *J. Phys. Chem. A.* **2007**, *111*, 1441–1451. (f) Xue, J.; Du, Y.; X. Guan, X.; Z. Guo, Z.; Phillips, D. L. *J. Phys. Chem. A* **2008**, *112*, 11582–11589.
(66) (a) Du, Y.; Ma, C.; Kwok, W. M.; Xue, J.; Phillips, D. L. *J. Org. Chem.* **2007**, *72*, 7148–7156. (b) Xue, J.; Du, Y.; Wang, J.; Platz, M. S.; Phillips, D. L. *J. Phys. Chem. A* **2008**, *112*, 1502–1510. (c) Xue, J.; Chan, P. Y.; Du, Y.; Guo., Z.; Chung, W. Y.; Toy, P. H.; Phillips, D. L. *J. Phys. Chem. B* **2007**, *111*, 12676–12684.
(67) Frisch, M. J.; Trucks, G. W.; Schlegel, H. B.; Scuseria, G. E.; Robb, M. A.; Cheeseman, J. R.; Zakrzewski, V. G.; Montgomery, J. A. Jr., Stratmann, R. E.; Burant, J. C.; Dapprich, S.; Millam, J. M.; Daniels, A. D.; Kudin, K. N.; Strain, M. C.; Farkas, O.; Tomasi, J.; Barone, V.; Cossi, M.; Cammi, R.; Mennucci, B.; Pomelli, C.; Adamo, C.; Clifford, S.; Ochterski, J.; Petersson, G. A.; Ayala, P. Y.; Cui, Q.; Morokuma, K.; Malick, D. K.; Rabuck, A. D.; Raghavachari, K.; Foresman, J. B.; Cioslowski, J.; Ortiz, J. V.; Baboul, A. G.; Stefanov, B. B.; Liu, G.; Liashenko, A.; Piskorz, P.; Komaromi, I.; Gomperts, R.; Martin, R. L.; Fox, D. J.; Keith, T.; Al-Laham, M. A.; Peng, C. Y.; Nanayakkara, A.; Gonzalez, C.; Challacombe, M.; Gill, P. M. W.; Johnson, B.; Chen, W.; Wong, M. W.; Andres, J. L.; Gonzalez, C.; Head-Gordon, M.; Replogle, E. S.; Pople, J. A. *Gaussian 98*; Gaussian, Inc., Pittsburgh, PA, 1998.
(68) (a) Hättig, C.; Weigend., F *J. Chem. Phys.* **2000**, *113*, 5154–5161. (b) Hättig, C.; Kőhn, A.; Hald, K. *J. Chem. Phys.* **2002**, *116*, 5401–5410. (c) Hättig, C. *J. Chem. Phys.* **2003**, *118*, 7751–7761.
(69) Olivucci, M. In *Computational Photochemistry*; Elsevier: Amsterdam, 2005; pp 92−128.
(70) Weigend, F.; Häser, F.; Patzelt, H.; Ahlrichs, R. *Chem. Phys. Lett.* **1998**, *294*, 143–152.
(71) (a) Ahlrichs, R.; Bär, M.; Häser, M.; Horn, H.; Kölmel, C. *Chem. Phys. Lett.* **1989**, *162*, 165.(b) For the current version of TURBOMOLE, see http://www.turbomole.de. (c) Treutler, O.; Ahlrichs, R. *J. Chem. Phys.* **1995**, *102*, 346.
(72) Frisch, M. J.; Trucks, G. W.; Schlegel, H. B.; Scuseria, G. E.; Robb, M. A.; Cheeseman, J. R.; Montgomery, J. A., Jr.; Vreven, T.; Kudin, K. N.; Burant, J. C.; Millam, J. M.; Iyengar, S. S.; Tomasi, J.; Barone, V.; Mennucci, B.; Cossi, M.; Scalmani, G.; Rega, N.; Petersson, G. A.; Nakatsuji, H.; Hada, M.; Ehara, M.; Toyota, K.; Fukuda, R.; Hasegawa, J.; Ishida, M.; Nakajima, T.; Honda, Y.; Kitao, O.; Nakai, H.; Klene, M.; Li, X.; Knox, J. E.; Hratchian, H. P.; Cross, J. B.; Bakken, V.; Adamo, C.; Jaramillo, J.; Gomperts, R.; Stratmann, R. E.; Yazyev, O.; Austin, A. J.; Cammi, R.; Pomelli, C.; Ochterski, J. W.; Ayala, P. Y.; Morokuma, K.; Voth, G. A.; Salvador, P.; Dannenberg, J. J.; Zakrzewski,

V. G.; Dapprich, S.; Daniels, A. D.; Strain, M. C.; Farkas, O.; Malick, D. K.; Rabuck, A. D.; Raghavachari, K.; Foresman, J. B.; Ortiz, J. V.; Cui, Q.; Baboul, A. G.; Clifford, S.; Cioslowski, J.; Stefanov, B. B.; Liu, G.; Liashenko, A.; Piskorz, P.; Komaromi, I.; Martin, R. L.; Fox, D. J.; Keith, T.; Al-Laham, M. A.; Peng, C. Y.; Nanayakkara, A.; Challacombe, M.; Gill, P. M. W.; Johnson, B.; Chen, W.; Wong, M. W.; Gonzalez, C.; and Pople, J. A. *Gaussian 03, Revision C.02*; Gaussian, Inc.: Wallingford, CT, 2004.

(73) Karlstrom, G.; Lindh, R.; Malmqvist, A.; Roos, B. O.; Ryde, U.; Veryazov, V.; Widmark, P.-O.; Cossi, M.; Schimmelpfennig, B.; Neogrady, P.; Seijo, L. *Comput. Mater. Sci.* **2003**, *28*, 222.

(74) (a) Burdzinski, G; Hackett, J. C.; Wang, J.; Gustafson, T. L.; Hadad, C. M.; Platz, M. S. *J. Am. Chem. Soc.* **2006**, *128*, 13402–13411. (b) Vyas, S.; Hadad, C. M.; Modarelli, D. A. *J. Phys. Chem. A* **2008**, *112*, 6533–6549. (c) Kucheryavy, P.; Li, Guifeng; Vyas, S.; Hadad, C. M.; Glusac, K. D. *J. Phys. Chem. A* **2009**, *113*, 6453–6461.(d) Vyas, S.; Hadad, C. M. In *Central Regional Meeting of American Chemical Society, 39th*; Covington, KY, United States, May 20−23 (2007).

(75) (a) Biswas, N.; Umapathy, S. *Chem. Phys. Lett.* **1995**, *236*, 24. (b) Biswas, N.; Umapathy, S. *J. Chem. Phys.* **1997**, *107*, 7849. (c) Biswas, N.; Umapathy, S. *Chem. Phys. Lett.* **1998**, *294*, 181. (d) Fujino, T.; Tahara, T. *J. Phys. Chem. A* **2000**, *104*, 4203.

(76) Platz, M. S. In *Reactive Intermediate Chemistry*; Moss, R. A, Platz, M. S., Jones, M. J., Eds.; Wiley-Interscience: Hoboken, NJ, 2004; Part 11.

(77) Schrader, B. *Raman/Infrared Atlas of Organic Compounds*; VCH: Weinheim, 1989.

(78) Johnson, W. T. G.; Sullivan, M. B.; Cramer, C. J. *Int. J. Quantum Chem.* **2001**, *85*, 492–508.